
ELSEVIER
International Journal of
HEAT and MASS
TRANSFER
Available online at www.sciencedirect.com
SciVerse ScienceDirect

International Journal of Heat and Mass Transfer 64 (2013) 212–223

Contents lists available at SciVerse ScienceDirect

International Journal of Heat and Mass Transfer

journal homepage: www.elsevier.com/locate/ijhmt

# Mixed convective flow and heat transfer of supercritical $CO_2$ in circular tubes at various inclination angles

Chuanyong Yang, Jinliang Xu *, Xiaodong Wang, Wei Zhang

*The Beijing Key Laboratory of Multiphase Flow and Heat Transfer, North China Electric Power University, Beijing 102206, PR China*

ARTICLE INFO

*Article history:*
Received 23 December 2012
Received in revised form 5 April 2013
Accepted 12 April 2013

*Keywords:*
Numerical simulation
Mixed convection
Supercritical $CO_2$
Heat transfer

ABSTRACT

We performed the numerical simulations of laminar mixed convective flow and heat transfer in a 0.5 mm diameter and 1000.0 mm length tube. The supercritical carbon dioxide in the tube was cooled at constant wall temperature. The inclination angles were in the range of −90° (vertical downward flow) to 90° (vertical upward flow). The velocity and temperature distributions, secondary flow, friction factor and heat transfer coefficient were plotted vs. inclination angles and gravity force magnitudes. The kinetic energy of secondary flow was introduced to quantify its effect on the heat transfer. It is found that under the mixed convective flow and heat transfer conditions, the horizontal flow display the largest heat transfer coefficients. The inclined flows at $\alpha = -30°$ and 30° also behave better heat transfer performance among various inclination angles. The effect of inclined angles on the heat transfer is decreased with decreases in the gravity force magnitudes. The combined parameter of $Gr/Re_b^2$ was used to quantify the buoyancy force effect on the flow and heat transfer.



## 1. Introduction

Supercritical fluids have wide applications in air-conditioners, nuclear reactors, supercritical fluid extraction due to their distinct physical properties. In modern power plants, heat is transferred to supercritical water. Rockets and military aircraft are cooled by fuel at supercritical pressures. Carbon dioxide is considered as a major alternative refrigerant for automotive air-conditioners and heat pump systems due to its good thermodynamic, transport, and environment properties [1]. It is also considered to be a possible working fluid for an Organic Rankine Cycle to recover low grade thermal energy. In order to develop compact heat exchangers, the channel hydraulic diameter is required to be smaller than 1.0 mm with $CO_2$ as the working fluid [2,3].

Great progress has been made on the flow and heat transfer with supercritical $CO_2$ in circular channels [4–9]. The test section was either vertically or horizontally positioned. Liao and Zhao [10–12] investigated the flow and heat transfer of supercritical $CO_2$ in vertical and horizontal tubes with inside diameters of 0.15–2.14 mm experimentally and numerically. The Reynolds number covered the range of $10^4$–$2 \times 10^5$. It is found that the effect of buoyancy force cannot be neglected even when the Reynolds number reached the value of $10^5$. The tube diameter has significant influence on the heat transfer. The Nusselt number is decreased with decreases in tube diameters, no matter for horizontal, upward and downward flows.

Jiang et al. [13–15] performed numerical and experimental studies on the flow and heat transfer of supercritical $CO_2$ in small diameter tubes. They analyzed effects of inlet temperatures, pressures, heat fluxes, flow directions, buoyancy force, and thermally induced flow acceleration on the convective heat transfer. The effect of tube wall thickness on the heat transfer was found to be weak, and the local heat transfer coefficients were decreased with increases in inlet pressures. The effect of buoyancy force is not important even at high heat fluxes with the tube diameters of 0.27 mm and 0.992 mm. The flow acceleration is the major reason to cause the abnormal heat transfer behavior. The numerical results show that there is no any turbulent flow model could give satisfactory results in comparison with experimental ones at this stage.

He et al. [16] numerically simulated the forced convection heat transfer of supercritical $CO_2$ in a 0.948 mm diameter tube using the low Reynolds number turbulent flow model. Even though there are some discrepancies between numerical and experimental results, the numerical simulations could reproduce the experimental phenomena. The effect of buoyancy force can be neglected for the forced convective heat transfer. The significant physical property variations and flow acceleration influence the heat transfer, to different degrees, causing the enhanced or deteriorated heat transfer.

The flow and heat transfer of supercritical $CO_2$ are very complex due to the significant change of physical properties. It is difficult to obtain the detailed flow structure in small diameter tubes by

* Corresponding author. Tel.: +86 10 61772268.
*E-mail address:* xjl@ncepu.edu.cn (J. Xu).

0017-9310/$ - see front matter 
http://dx.doi.org/10.1016/j.ijheatmasstransfer.2013.04.033

**Nomenclature**

| | |
|---|---|
| $A$ | top generatrix point |
| $A_c$ | cross section area of the tube, $m^2$ |
| $B$ | bottom generatrix point |
| $C_f$ | finning fraction factor |
| $d$ | tube diameter, m |
| $e$ | enthalpy, J/kg |
| $g$ | gravity force, $m/s^2$ |
| $Gr$ | Grashof number |
| $h$ | heat transfer coefficient, $W/m^2$ K |
| $k_1$ | kinetic energy of secondary flow, $m^2/s^2$ |
| $L$ | tube length, m |
| $m$ | mass flow rate, kg/s |
| $Nu$ | Nusselt number |
| $p$ | pressure, Pa |
| $q$ | heat flux, $W/m^2$ |
| $r$ | radial coordinate, m |
| $R$ | tube radius, m |
| Re | Reynolds number |
| $T$ | temperature, K |
| $T_{pc}$ | pseudocritical temperature, K |
| $u$, $v$, $w$ | velocity of $x$, $y$, $z$ direction, m/s |
| $x$, $y$, $z$ | Cartesian coordinate |

*Greek symbols*

| | |
|---|---|
| $\alpha$, $\theta$ | angle, ° |
| $\lambda$ | thermal conductivity, W/m K |
| $\mu$ | dynamic viscosity, Pa s |
| $\rho$ | density, $kg/m^3$ |
| $\tau$ | shear stress, $N/m^2$ |

*Subscripts*

| | |
|---|---|
| b | bulk fluid |
| in | inlet condition |
| pc | pseudocritical |
| w | wall |

experiments, but this can be done by computational fluid dynamics (CFD) simulations. Du et al. [17] used the commercial software FLUENT to simulate heat transfer of supercritical $CO_2$ in a 6 mm diameter tube for the cooling boundary conditions. Almost all the turbulent flow models could predict the heat transfer trend. The low Reynolds number turbulent flow model gave the best results among various turbulent flow models. With continuous decreases in the bulk fluid temperatures, the buoyancy force is increased, attains the maximum value at the pseudocritical temperature, and then decreased, resulting in great effect on the convective heat transfer in tubes.

Cao et al. [2] numerically simulated the laminar heat transfer of supercritical $CO_2$ in horizontally circular and triangular channels with cooling boundary conditions. The effects of fluid physical properties and channel geometries on the heat transfer were analyzed. The buoyancy force could enhance heat transfer near the pseudocritical temperature region. The effect of secondary flow on the heat transfer was analyzed qualitatively.

Great progress has been made on the convective heat transfer in inclined tubes. ORFI [18] numerically simulated the laminar mixed convective heat transfer of air and water in inclined tubes. The buoyancy force induced secondary flow was analyzed. The secondary flow induced by air flowing in tubes is much stronger than that caused by water flowing in tubes. The secondary flow is weakened with increases in inclination angles, and enhanced with increases in the Grashof number. The average Nusselt number was increased by increasing the Grashof number for any inclination angles. There is an optimal inclination angle to reach a maximum Nusselt number for a specific working fluid and Grashof number.

Walisch et al. [19] experimentally investigated the mixed turbulent heat transfer of supercritical $CO_2$ in horizontal, vertical and inclined tubes. The results show that the large thermal capacity of $CO_2$ enhances heat transfer for any Reynolds number and inclination angle. The heat transfer is enhanced by the buoyancy force for the Reynolds number smaller than $10^4$, sensitive to the inclination angles for Reynolds number in the range of $10^4$ to $7 \times 10^4$, and not influenced by the buoyancy force for Reynolds number larger than $7 \times 10^4$. Busedra et al. [20] experimentally investigated the laminar mixed convective heat transfer in half circular tube using water as the working fluid. The inclination angles and Reynolds number were in the range of $-20°$ to $20°$ and 500–1500, respectively. The heat transfer is influenced by the Grashof number, Reynolds number and inclination angle for the downward flow with inclination angles of $-20°$–$0°$. The heat transfer is mainly affected by the Grashof number for the upward flows with inclination angles of $0°$–$20°$. Ozsuanr et al. [21] experimentally studied the mixed convective heat transfer in horizontal and upward rectangular ducts with inclination angles of $0°$–$30°$ and Reynolds numbers of 50–1000. The heat transfer performance can be improved by increasing the inclination angles. Mohammed et al. [22] experimentally investigated the mixed convective heat transfer of air flowing in inclined circular tubes. The results demonstrate that the Nusselt numbers were increased by raising the heat fluxes and decreased with increases in inclination angles. Chong et al. [23] investigated the laminar mixed convective heat transfer of air flowing in inclined tubes. The optimal inclination angles to reach the maximum heat transfer coefficient were decreased from $30°$ to $-30°$ with Reynolds number increased from 420 to 1720. With continuous increases in inclination angles, the heat transfer coefficients were increased, attained the maximum value and then decreased. The inclination angles have mini influence on the heat transfer coefficients at high Reynolds number.

The above literature survey shows that most studies focused on the investigations of air and water flowing in inclined tubes. Less studies have been performed for supercritical $CO_2$ flowing in inclined tubes. The objective of this study is to investigate the laminar mixed convective heat transfer of supercritical $CO_2$ flowing in tubes with inclination angles of $-90°$ to $90°$. The optimal inclination angles were identified for the laminar mixed convective heat transfer to have maximum heat transfer coefficients. The secondary flow mechanism and its intensity were analyzed. The effects of various parameters such as gravity force, inlet Reynolds number as well as wall temperatures on the mixed convective heat transfer were obtained. This study provides the guidelines for design and operation of compact heat exchanges using supercritical $CO_2$ as the working fluid.

## 2. Numerical simulations

### 2.1. Physical configuration and governing equations

Evaporator and condenser are key components of air-conditioners. Compact heat exchangers with $CO_2$ as the working fluid run at high pressures. Air-conditioner for vehicles is one of the example applications. Capillary tube with diameters of a couple of millimeters is attractive for such applications. This is because the capillary

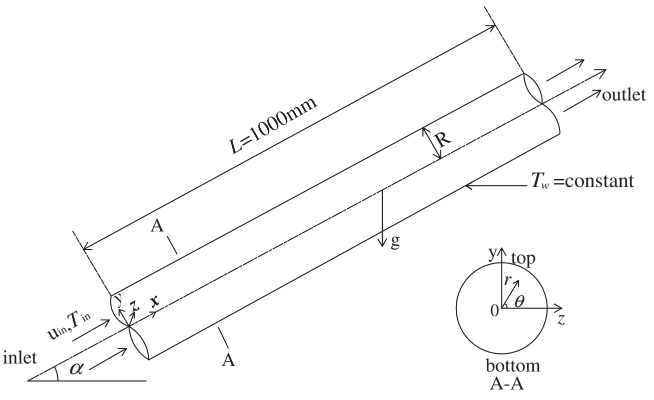


**Fig. 1.** Physical configuration and coordinate system.

tube has high heat transfer coefficients and thin metal wall thickness can be used to sustain high pressures. Laminar flow can be ensured due to the miniature or microchannels used.

The supercritical $CO_2$ in the tube was cooled at the constant wall temperature. The problem is a steady three-dimensional laminar flow. Fig. 1 shows the physical configuration and coordinate. The tube had a diameter of $d = 0.5$ mm and length of $L = 1000$ mm. The circumferential angle was recorded as $\theta$. The tube inclination angle was $\alpha$, having the range of $-90°$ to $90°$, in which $\alpha = 90°$, $0°$ and $-90°$ referring to the vertical upward flow, horizontal flow and vertical downward flow, respectively. The gravity force can be decomposed into the $x$-component and $y$-component. The $\theta = 90°$ and $-90°$ refer to the top generatrix and bottom generatrix, respectively. The governing equations are:

Mass conservation equation:

$$\frac{\partial(\rho u)}{\partial x} + \frac{\partial(\rho v)}{\partial y} + \frac{\partial(\rho w)}{\partial z} = 0 \tag{1}$$

Momentum conservation equations:

$$\frac{\partial(\rho uu)}{\partial x} + \frac{\partial(\rho vu)}{\partial y} + \frac{\partial(\rho wu)}{\partial z} = \frac{\partial}{\partial x}\left(\mu\frac{\partial u}{\partial x}\right) + \frac{\partial}{\partial y}\left(\mu\frac{\partial u}{\partial y}\right) + \frac{\partial}{\partial z}\left(\mu\frac{\partial u}{\partial z}\right) - \frac{\partial p}{\partial x} - \rho g \sin\alpha \tag{2}$$

$$\frac{\partial(\rho uv)}{\partial x} + \frac{\partial(\rho vv)}{\partial y} + \frac{\partial(\rho wv)}{\partial z} = \frac{\partial}{\partial x}\left(\mu\frac{\partial v}{\partial x}\right) + \frac{\partial}{\partial y}\left(\mu\frac{\partial v}{\partial y}\right) + \frac{\partial}{\partial z}\left(\mu\frac{\partial v}{\partial z}\right) - \frac{\partial p}{\partial y} + \rho g \cos\alpha \tag{3}$$

$$\frac{\partial(\rho uw)}{\partial x} + \frac{\partial(\rho vw)}{\partial y} + \frac{\partial(\rho ww)}{\partial z} = \frac{\partial}{\partial x}\left(\mu\frac{\partial w}{\partial x}\right) + \frac{\partial}{\partial y}\left(\mu\frac{\partial w}{\partial y}\right) + \frac{\partial}{\partial z}\left(\mu\frac{\partial w}{\partial z}\right) - \frac{\partial p}{\partial z} \tag{4}$$

Energy conservation equation:

$$\frac{\partial(\rho ue)}{\partial x} + \frac{\partial(\rho ve)}{\partial y} + \frac{\partial(\rho we)}{\partial z} = \frac{\partial}{\partial x}\left(\lambda\frac{\partial T}{\partial x}\right) + \frac{\partial}{\partial y}\left(\lambda\frac{\partial T}{\partial y}\right) + \frac{\partial}{\partial z}\left(\lambda\frac{\partial T}{\partial z}\right) \tag{5}$$

The bulk mean temperature is defined as

$$T_b = \int_{A_c} \rho u T dA \Big/ \int_{A_c} \rho u dA \tag{6}$$

The bulk mean Reynolds number is defined according to the physical properties of the bulk mean temperature

$$Re_b = \frac{\rho_b u_b d}{\mu_b} \tag{7}$$

The heat flux at the wall is calculated by

$$q_w = -\lambda_w \left(\frac{\partial T}{\partial r}\right)_w \tag{8}$$

The local heat transfer coefficient is defined as

$$h = \frac{q_w}{T_w - T_b} \tag{9}$$

The local Nusselt number is

$$Nu_w = \frac{hd}{\lambda_b} \tag{10}$$

### 2.2. Grid generations and boundary conditions

The commercial software FLUENT 6.3 simulates the three-dimensional problem. The control volume method treats the mass, momentum and energy conservation equations. The model shall consider the buoyancy force and secondary flow. Grid generation and size are important for the numerical simulations. The refined grids were adopted near the wall to deal with the great velocity and temperature gradients. The final grid number was 0.6 million using hexahedral unstructured grids. Further refinement of grids yields no apparent improvement of the computation results. Velocity and temperature are assumed uniform at the tube inlet. The free outflow boundary condition was applied at the tube outlet.

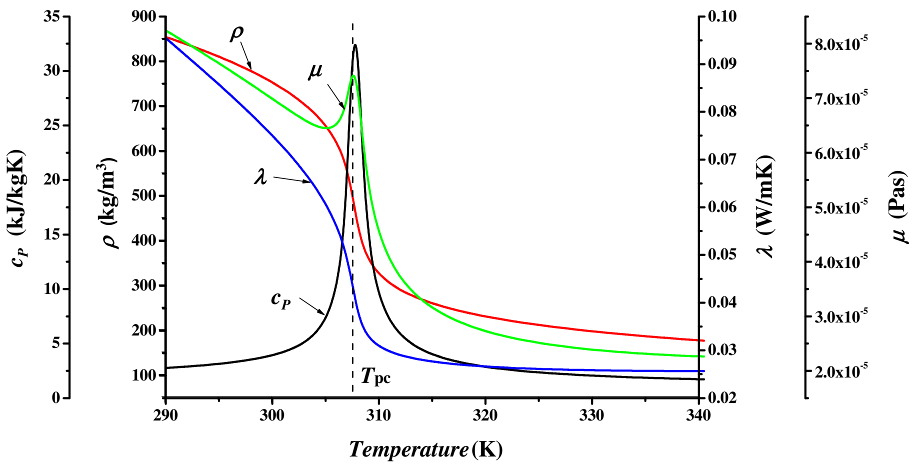


**Fig. 2.** Physical properties of $CO_2$ at 8.0 MPa.

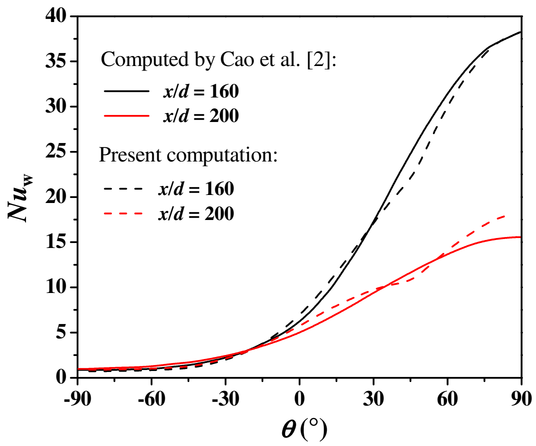


Fig. 3. Comparison of the present numerical simulation with that of Cao et al. [2].

The no-slip boundary condition was applied on the wall. The tube was cooled by the constant wall temperature of $T = T_w$.

The implicit-double-accuracy-solver computes the steady three-dimensional laminar problem. The SIMPLEC method treated the pressure and velocity coupling. The skewness correction value was set as one. The second-order-upwind scheme was applied to solve the momentum and energy equations. The under-relaxation factor was set as the default value to reach fast convergence. The solution was assumed to be convergent when the residual errors are smaller than $1.0 \times 10^{-6}$ for mass conservation equation and $1.0 \times 10^{-8}$ for momentum and energy conservation equations. Under such circumstances, the mass flow rates at the tube inlet and outlet are exactly equal. The outlet temperature and the residual error curve do not change any more.

The computational time and cost shall be considered during the numerical simulations. Regarding Fig. 1, the geometry configuration is symmetric against the Y direction, thus only half of the computational domain is enough. We did not use the symmetric boundary condition against Y. Instead, the whole computation domain (the entire cross section of the tube) was applied to perform the computations. Each case needs about a couple of hours, which is acceptable for the numerical simulations.

Fig. 2 shows thermal capacities, thermal conductivities, dynamic viscosities and densities of supercritical $CO_2$ at a pressure of $p = 8.0$ MPa. The physical properties were cited from the NIST

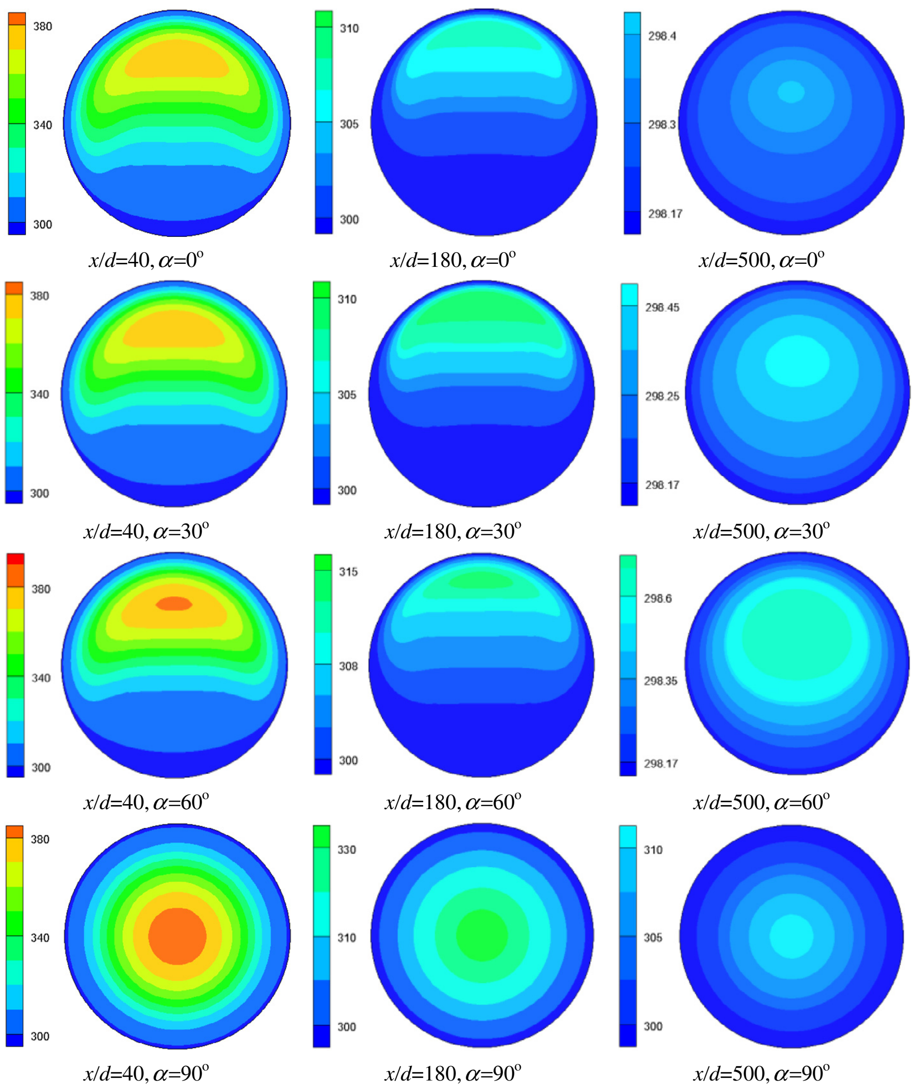


Fig. 4. Temperature contours vs. inclination angles ($\alpha = 0°$, $30°$, $60°$ and $90°$) at various axial locations for run 1.

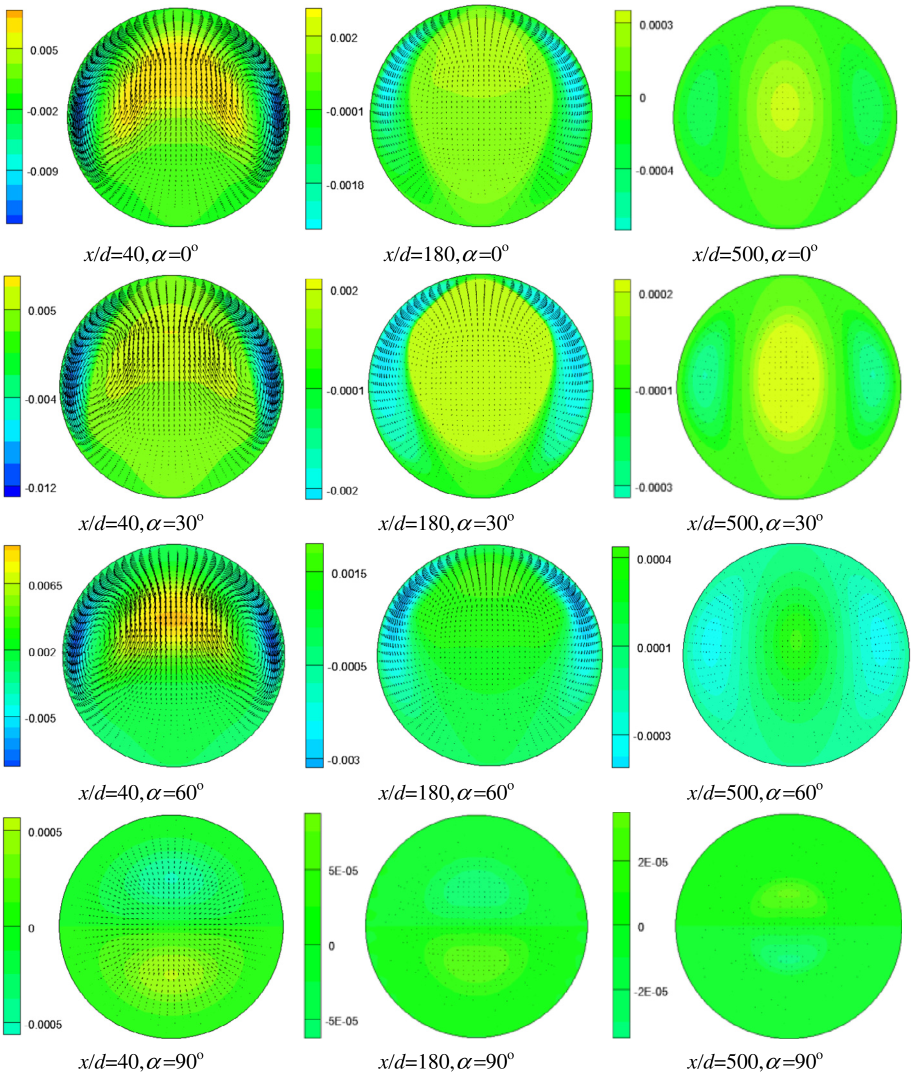


**Fig. 5.** Flow contours vs. inclination angles ($\alpha$ = 0°, 30°, 60° and 90°) at various axial locations for run 1.

Standard Reference Database 23 (REFPROP Version8.0) [24]. The thermal capacity reached the maximum value at the temperature of 307.6 K (identified as the pseudocritical temperature, $T_{pc}$). The physical properties had significant changes near the pseudocritical temperature. The varied physical properties of $CO_2$ are incorporated in the computation via the piecewise-liner input.

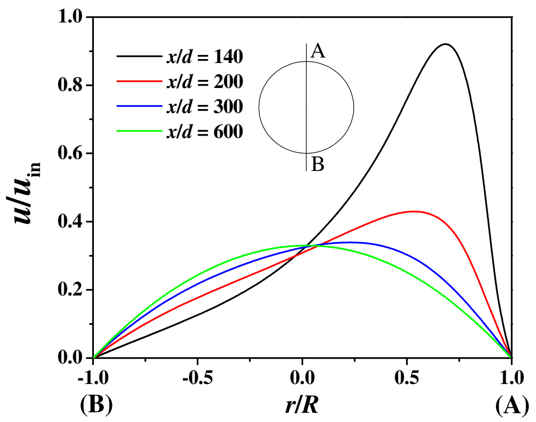


**Fig. 6.** Axial velocities vs. radial coordinate at various axial locations for run 2 ($p$ = 8.0 MPa, $\alpha = 30^{\circ}$).

## 3. Result and discussion

### 3.1. The temperature and velocity fields

The following parameters of $p$ = 8.0 MPa, $T_{in}$ = 393.15 K, $m_{in} = 1.6 \times 10^{-5}$ kg/s and $T_w$ = 298.15 K were set for the present

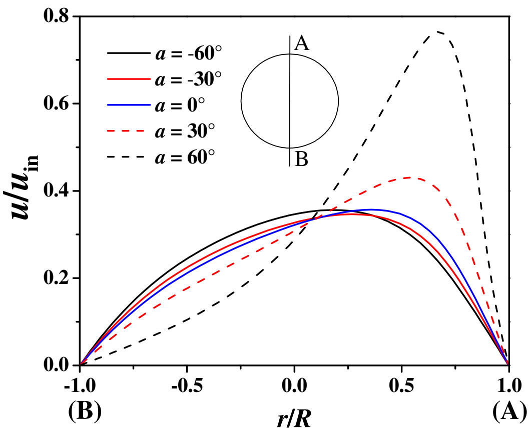


**Fig. 7.** Effect of inclination angles on the axial velocities at $x/d$ = 200 for run 2 ($p$ = 8.0 MPa).

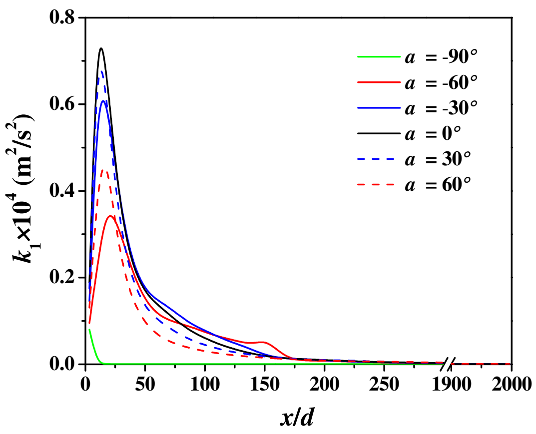


**Fig. 8.** Kinetic energy of secondary flow ($k_1$) vs. axial locations at various inclination angles for run 2 ($p$ = 8.0 MPa).

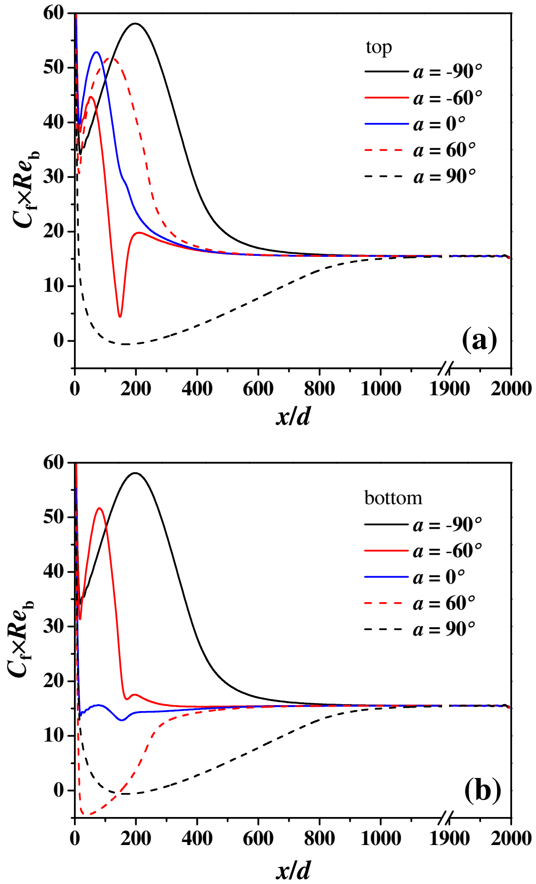


**Fig. 9.** Friction factors vs. axial coordinates at various inclination angles for run 2 ($p$ = 8.0 MPa, a: top generatrix point, b: bottom generatrix point).

numerical simulations. Fig. 3 plotted the local Nusselt numbers vs. the circumferential angles at two axial locations. It is seen that our present numerical simulations agree well with those reported by Cao et al. [2]. Fig. 4 illustrates the temperature contours at three axial locations of $x/d$ = 40, 180 and 500 and four inclination angles ($\alpha$ = 0°, 30°, 60° and 90°) for run 1 (see Table 1 for run parameters). The vertical upward flow ($\alpha$ = 90°) behaves a set of concentric circles for temperature contours. The temperature contours are severely distorted for the inclined flows. The temperatures are

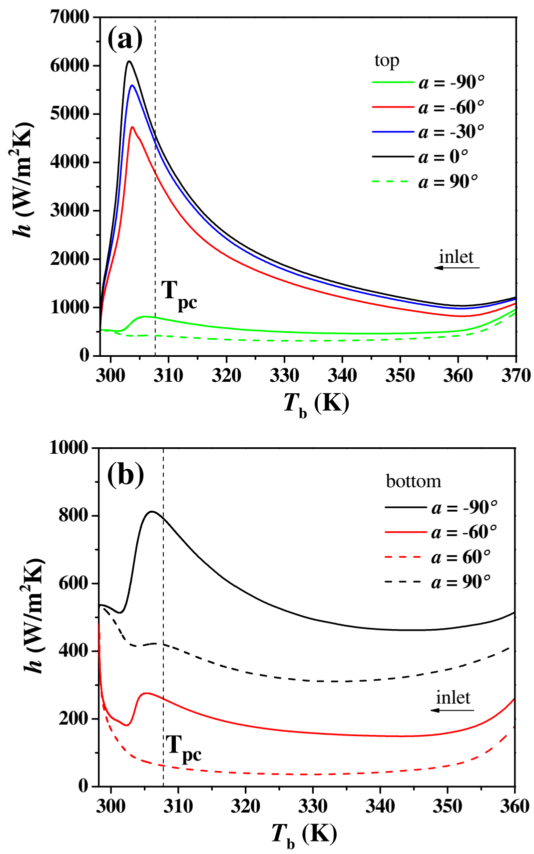


**Fig. 10.** Heat transfer coefficients vs. bulk fluid temperatures at various inclination angles for run 2 ($p$ = 8.0 MPa, a: top generatrix point, b: bottom generatrix point).

higher at the upper part of the tube cross section, and decreased gradually toward the wall. The distortion of the temperature contours became weak with fluid flowing downstream. The temperature contours approach the concentric circles at $x/d$ = 500 for any inclination angles (see Fig. 4).

Fig. 5 shows the flow contours at four inclination angles ($\alpha$ = 0°, 30°, 60° and 90°) and three axial locations ($x/d$ = 40, 180 and 500). Certainly there is no secondary flow for vertical upward flow ($\alpha$ = 90°). Inclined flows result in apparent secondary flow near the tube entrance ($x/d$ = 40), under which vortex can be observed. The secondary flow intensity is weakened when the $CO_2$ fluid flows downstream. The gravity force can be decomposed into components along the axial flow direction and radial direction for inclined flows. For the wall cooled at temperature $T_w$, the $CO_2$ fluid is heavier close to the wall but lighter in the upper part of the cross section. The secondary flow is generated by the density difference over the tube cross section, ensuring the downward flow along the tube wall and upward flow in the center part of the cross section. Vortex is created when the upward flow meets with the downward flow. The heat transfer is enhanced by the secondary flow near the wall. There is no radial-component of the gravity force for the vertical flow, yielding no secondary flow at $\alpha$ = 90°. The secondary flow intensity is enhanced when the bulk $CO_2$ temperature reaches the pseudocritical temperature, at which the $CO_2$ density is very sensitive to the mini changes of temperatures. With fluid flowing downstream, the fluid temperatures are below the pseudocritical temperature, shortening the temperature difference between the fluid and wall to yield the decreased secondary flow intensity.

Fig. 6 shows the axial velocities ($u/u_{in}$) vs. the radial coordinate ($r/R$) along the $AB$ line. The location of $r/R$ = 1.0 and $r/R$ = −1.0 represent the top generatrix $A$ and the bottom generatrix $B$ respec-

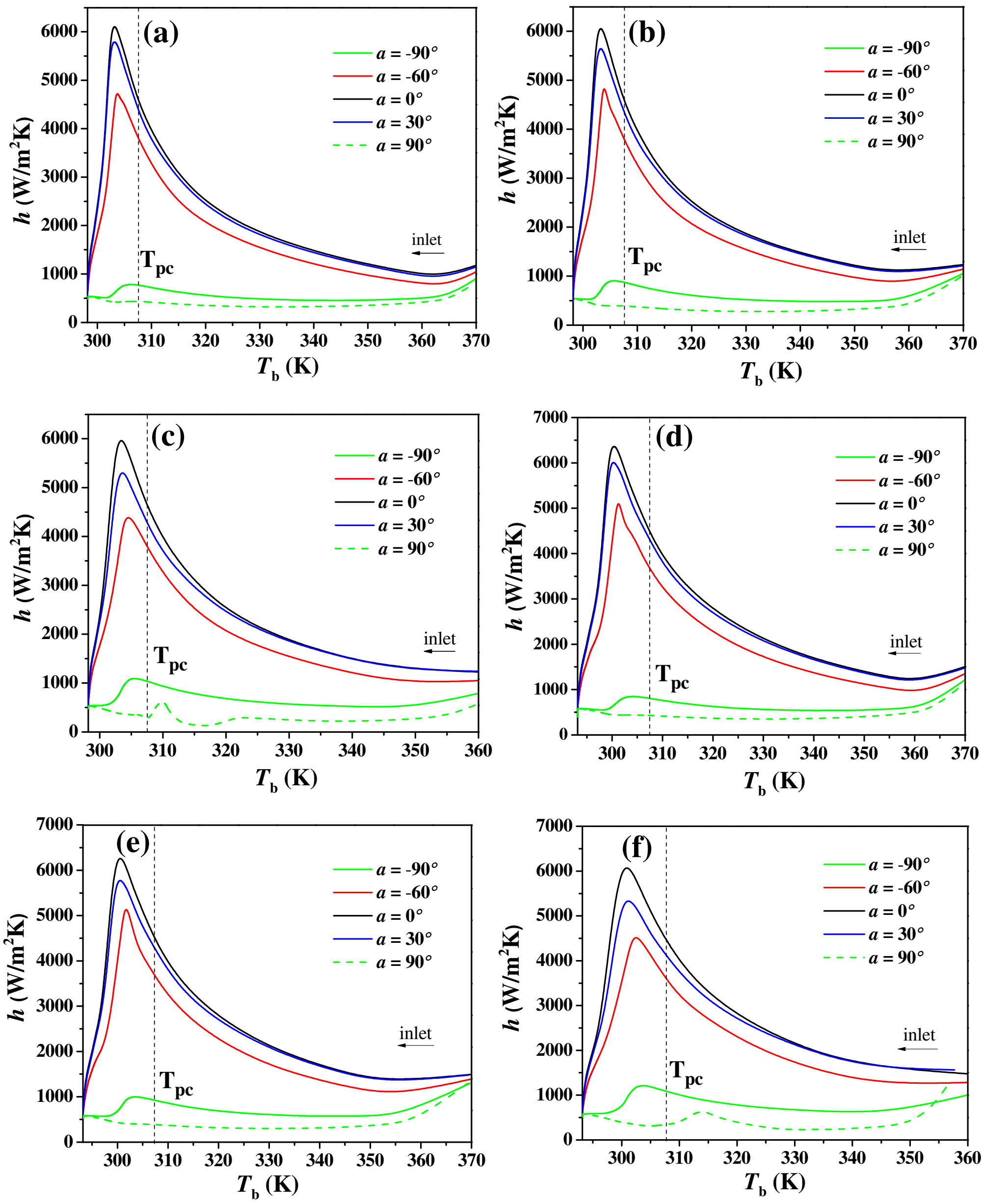


**Fig. 11.** Heat transfer coefficients at the top generatrix point vs. bulk fluid temperatures at various inclination angles (a: run 1, b: run 3, c: run 4, d: run 5, e: run 6, f: run 7).

tively. These velocities were plotted at four axial locations of $x/d$ = 140, 200, 300 and 600. Because the $CO_2$ density is increased along the tube, $u/u_{in}$ is always smaller than unity. The axial velocities are not symmetric vs. the radial coordinate $r$, which are larger at the upper part of the tube ($0 < r/R < 1.0$) than those at the lower part of the tube ($-1.0 < r/R < 0$). This is especially apparent at the tube entrance (see the curves of $x/d$ = 140 and 200). When the flow is far away from the tube entrance, the velocity profiles approach the parabolic curves (see the curves of $x/d$ = 300 and 600). The distortion of velocity profiles is weakened with flow development.

Fig. 7 considers the effect of inclination angles on the axial velocity distributions. Five inclination angles of $\alpha = -60°$, $-30°$, 0°, 30° and 60° were demonstrated. The axial velocity profiles are less distorted and behave small differences for $\alpha = -60°$, $-30°$, 0° (inclined downward and horizontal flows). However, the axial velocities are severely distorted for the inclined upward flows ($\alpha$ = 30° and 60°). The peak axial velocity appears between the tube center ($r/R = 0$) and the top generatrix $A$ at $r/R = 1.0$.

Gessner et al. [25] analyzed the secondary flow mechanism in the rectangular corner for turbulent flow. To the authors' knowledge, the quantitative analysis of the secondary flow cannot be found in the open literature. Here the kinetic energy of the secondary flow is introduced to quantify the secondary flow intensity, which is expressed as

$$k_1 = \frac{1}{A_c} \int_{A_c} (v^2 + w^2) dA \tag{11}$$

where the kinetic energy $k_1$ has the unit of $m^2/s^2$.

Fig. 8 shows the kinetic energies of secondary flow vs. axial coordinate for various inclination angles. The kinetic energies of secondary flow can be neglected for the downstream flow of $x/d > 200$. They are almost zero for the vertical upward and downward flows ($\alpha$ = 90° and $-90°$), at which there is no component of gravity force perpendicular to the axial flow direction to create the secondary flow. The kinetic energies are increased, attain the

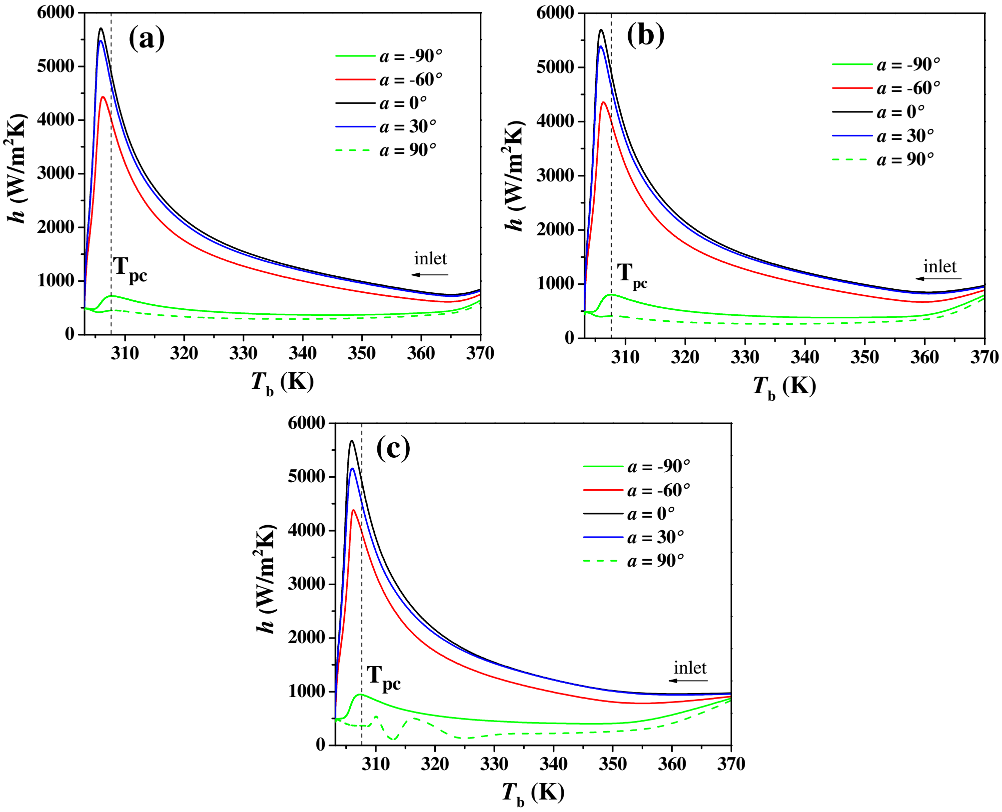


**Fig. 12.** Heat transfer coefficients at the top generatrix point vs. bulk fluid temperatures at various inclination angles (a: run 8, b: run 9, c: run 10).

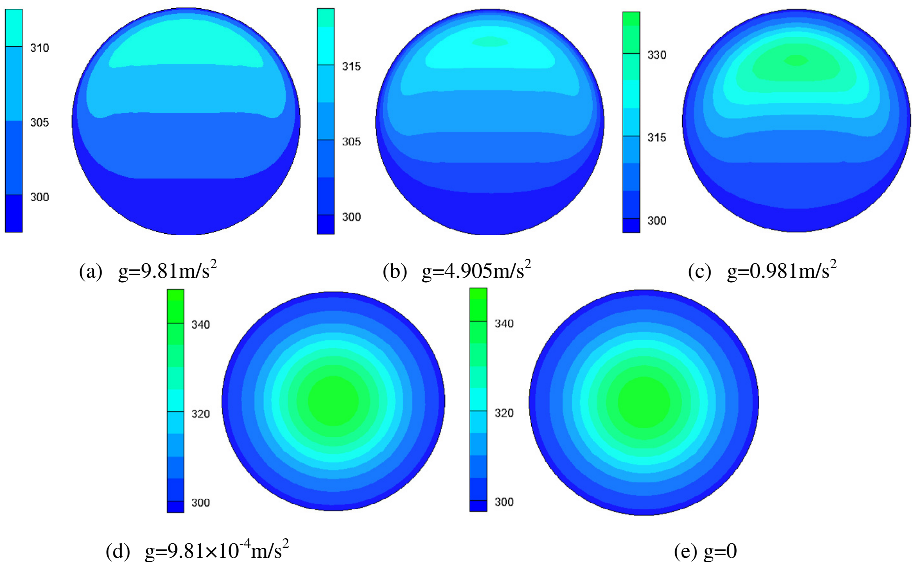


**Fig. 13.** Effect of gravity force magnitude on temperature contours at $x/d = 120$ for inclination angle $\alpha = 0°$ (a: run 2, b: run 11, c: run 12, d: run 13, e: run 14).

maximum value at the horizontal flow ($\alpha = 0°$) and then decreased, with increases in inclination angles from $-60°$ to $60°$. For the horizontal flow the total gravity force is acted over the tube cross section thus the secondary flow intensity is maximized.

### 3.2. The Finning friction factor and heat transfer coefficient

The local Finning friction factor $C_f$ is defined as

$$C_f = \frac{\tau_w}{\frac{1}{A_c}\int_{A_c} \frac{1}{2}\rho u^2 dA} \tag{12}$$

where $\tau_w$ is the shear stress on the wall, which is expressed as $\tau_w = -\mu_w(\partial u/\partial r)_w$. This study used $C_f \times Re_b$ instead of $C_f$.

Fig. 9 shows the $C_f \times Re_b$ curves along the axial coordinate ($x/d$) at various inclination angles, in which Fig. 9a and b for the top generatrix point *A* and bottom generatrix point *B*, respectively. The $C_f \times Re_b$ values do not change and reach 16 for $x/d > 1000$, corresponding to that for the fully developed laminar convective flow in circular tubes, consistent with the classical solution [2]. The $C_f \times Re_b$ behaves significant changes for $x/d < 1000$. For the vertical downward flow ($\alpha = -90°$), the fluid in the tube core is lighter thus the buoyancy force is upward, decreasing the down-

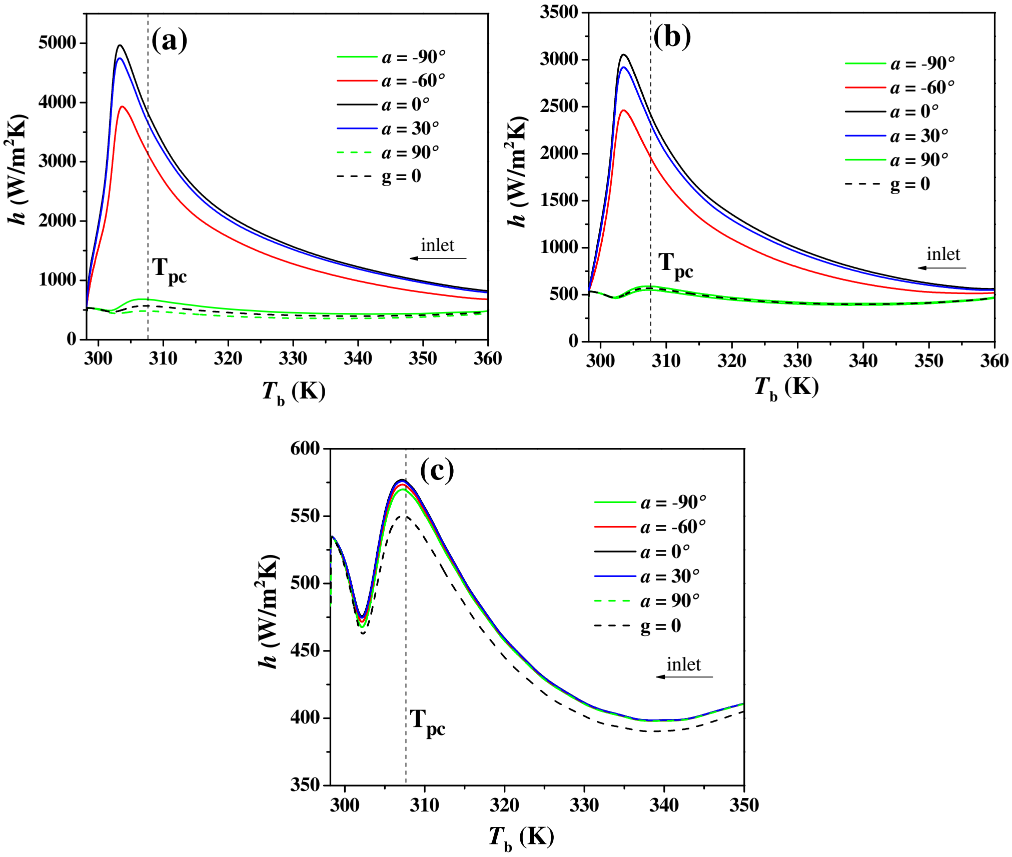


**Fig. 14.** Heat transfer coefficients at the top generatrix point vs. bulk fluid temperatures at various inclination angles (a: run 11, b: run 12, c: run 13).

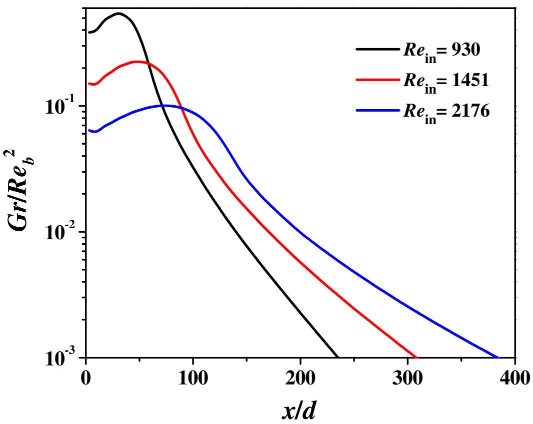


**Fig. 15.** The $Gr/Re_b^2$ vs. inlet Reynolds numbers along the axial coordinate for runs 5–7 ($\alpha = 0°$).

ward flow velocity in the bulk region but increasing the fluid velocity and its gradient near the wall. This explains the reason that the vertical downward flow behaves the maximum $C_f \times Re_b$ values among various inclination angles. On the other hand, for the vertical upward flow ($\alpha = 90°$), the upward buoyancy force accelerates the fluid velocities in the core region but decreases the fluid velocities near the wall, yielding the smallest $C_f \times Re_b$ among various inclination angles. Under specific conditions the fluid velocity becomes negative near the wall, causing the negative $C_f \times Re_b$ near the wall. At the bottom generatrix point $B$, $C_f \times Re_b$ is decreased with continuous increases in inclination angles.

Fig. 10 illustrates the heat transfer coefficients vs. bulk fluid temperatures at various inclination angles. The following phenomena can be identified: (a) With continuous decreases in bulk fluid temperatures, heat transfer coefficients are slightly decreased at the tube entrance, continuously increased until maximum heat transfer coefficients are reached at the bulk temperature slightly smaller than the pseudocritical temperature $T_{pc}$. Then the heat transfer coefficients are further decreased. The variation of heat transfer coefficients is consistent with the trend reported by Refs. [26–28]. (b) The heat transfer coefficients at the top generatrix point $A$ are several times larger than those at the bottom generatrix point $B$. This is due to the stratified fluid structure over the tube cross section. The lighter fluid at the top part of the tube cross section yields the enhanced heat transfer at the top generatrix location. (c) The horizontal flow ($\alpha = 0°$) behaves the maximum heat transfer coefficients at the top generatrix point. This is due to the fact that the horizontal tube creates the strongest secondary flow over the tube cross section. Slightly inclined downward flows also have better heat transfer performance.

In order to verify the effect of running parameters on the heat transfer characteristics, we plotted the heat transfer coefficients vs. bulk fluid temperatures for various inclination angles in Figs. 11 and 12. Nine runs were selected (see Table 1 for runs 1 and 3–10). These variations of heat transfer coefficients do coincide with those given in Fig. 10. The horizontal flow ($\alpha = 0°$) or slightly inclined flow ($\alpha = 30°$ or $-30°$) displays the better heat transfer performance, providing the guidelines for the design and operation of compact heat exchangers. This trend of heat transfer coefficients is consistent with the secondary flow and its intensity shown in previous figures.

Fig. 13 demonstrates the effect of gravity force magnitude on the temperature contours at the tube entrance ($x/d = 120$). Five

**Table 1**
Run parameters for the present computations.

| Cases | $m_{in}$ (kg/s) | $T_w$ (K) | $Re_{in}$ | $g$ (m/s$^2$) | $\alpha$ (°) | $p$ (MPa) |
|---|---|---|---|---|---|---|
| Run 1 | $1.8 \times 10^{-5}$ | 298.15 | 2176 | 9.81 | −90°–90° | 8.0 |
| Run 2 | $1.6 \times 10^{-5}$ | 298.15 | 1934 | 9.81 | −90°–90° | 8.0, 9.0, 10.0 |
| Run 3 | $1.2 \times 10^{-5}$ | 298.15 | 1451 | 9.91 | −90°–90° | 8.0 |
| Run 4 | $7.7 \times 10^{-6}$ | 298.15 | 930 | 9.81 | −90°–90° | 8.0 |
| Run 5 | $1.8 \times 10^{-5}$ | 293.15 | 2176 | 9.81 | −90°–90° | 8.0 |
| Run 6 | $1.2 \times 10^{-5}$ | 293.15 | 1451 | 9.81 | −90°–90° | 8.0 |
| Run 7 | $7.7 \times 10^{-6}$ | 293.15 | 930 | 9.81 | −90°–90° | 8.0 |
| Run 8 | $1.8 \times 10^{-5}$ | 303.15 | 2176 | 9.81 | −90°–90° | 8.0 |
| Run 9 | $1.2 \times 10^{-5}$ | 303.15 | 1451 | 9.81 | −90°–90° | 8.0 |
| Run 10 | $7.7 \times 10^{-6}$ | 303.15 | 930 | 9.81 | −90°–90° | 8.0 |
| Run 11 | $1.6 \times 10^{-5}$ | 298.15 | 1934 | 4.905 | −90°–90° | 8.0 |
| Run 12 | $1.6 \times 10^{-5}$ | 298.15 | 1934 | 0.981 | −90°–90° | 8.0 |
| Run 13 | $1.6 \times 10^{-5}$ | 298.15 | 1934 | $9.81 \times 10^{-4}$ | −90°–90° | 8.0 |
| Run 14 | $1.6 \times 10^{-5}$ | 298.15 | 1934 | 0 | 0° | 8.0 |

Note: The $CO_2$ inlet temperature is $T_{in}$ = 393.15 K for all the cases. The range of −90°–90° represents the inclination angles of −90°, −60°, −30°, 0°, 30°, 60° and 90°.

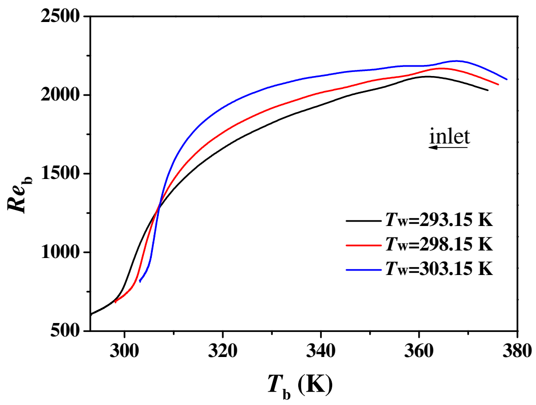


**Fig. 16.** Reynolds number vs. bulk fluid temperatures at various wall temperatures for runs1, 5 and 8 ($\alpha = 0^{\circ}$).

gravity forces were used for comparison. Temperatures show non-uniform distribution over the tube cross section at $g$ = 9.81 m/s$^2$ (earth level) and 4.905 m/s$^2$. This behavior is still apparent at $g$ = 0.981 m/s$^2$, which is one-tenth of the earth level. Generally, temperatures are higher at the upper part of the tube cross section under such circumstances. Temperature contours show a set of concentric circles at micro ($g = 9.81 \times 10^{-4}$ m/s$^2$) and zero gravity environment. We also note that temperatures in the tube core are higher at the micro or zero gravity environment than those at larger gravity forces. The micro or zero gravity forces result in weak or no buoyancy force and secondary flow over the tube cross section to yield poor heat transfer.

Fig. 14 illustrates the effect of gravity forces on heat transfer coefficients at the top generatrix point, in which Fig. 14a for $g$ = 4.905 m/s$^2$ (half of the ground level), 14b for $g$ = 0.981 m/s$^2$ (one-tenth of the ground level) and 14c for $g = 9.81 \times 10^{-4}$ m/s$^2$ (micro gravity). In each subfigure, heat transfer coefficients were also plotted for zero gravity ($g$ = 0). The horizontal flow or the inclined flow behaves much higher heat transfer coefficients than those for vertical upward or downward flows at $g$ = 4.905 m/s$^2$ (see Fig. 14a) and 0.981 m/s$^2$ (see Fig. 14b). Heat transfer coefficients for vertical flows at larger gravity force level are quite close to those at zero gravity force. At larger gravity force the buoyancy force has neglectable effect on the heat transfer and the secondary flow cannot be generated for vertical flows. Fig. 14c demonstrates that the micro and zero gravity forces behave similar heat transfer performance for any inclination angles.

The Grashof number is introduced to quantify the buoyancy force effect on the flow and heat transfer:

$$Gr = \frac{gd^3(\rho_w - \rho_b)\rho_b}{\mu_b^2} \tag{13}$$

When supercritical fluids in tubes are cooled at constant wall temperature, the fluid temperatures are continuously decreased to cause the density variation along the flow direction. The density changes near the pseudocritical temperature region are significant. The thermal induced density variation may cause the secondary flow over the tube cross section under horizontal or inclined flows, affecting the heat transfer coefficient magnitude and distribution.

Many heat transfer handbooks discuss the mixed convective flow and heat transfer in straight channels [29]. The combined parameter of $Gr/Re_b^2$ quantifies the effect of buoyancy force on the heat transfer. Usually, the mixed convective flow is important when $Gr/Re_b^2$ was in a range of $C_{min}$ and $C_{max}$, where $C_{min}$ is the critical minimal $Gr/Re_b^2$ below which the flow approaches the forced convective flow, and $C_{max}$ is the critical maximum $Gr/Re_b^2$ above which the flow approaches the pure free convective flow. For commonly used fluids such as water or air flowing in ducts, the mixed convective flow occurs with $0.1 < Gr/Re_b^2 < 10$ [29]. The working fluids may influence the two critical limit values. Cao et al. [2] and Du et al. [17] noted that the mixed convective flow effect is significant for $10^{-3} < Gr/Re_b^2 < 10^{-2}$ with $CO_2$ as the working fluid. Fig. 15 gave the $Gr/Re_b^2$ variations along the axial coordinate ($x/d$) for horizontal flows. Three inlet Reynolds numbers were selected for the presentation. It is seen that $Gr/Re_b^2$ is increased at the tube entrance, attains the maximum value and then decreased along the flow direction. The locations at which $Gr/Re_b^2$ reached $10^{-3}$ depend on the inlet Reynolds number. For example, $Gr/Re_b^2$ reached $10^{-3}$ at $x/d$ = 235 for $Re_{in}$ = 930 but this happens at $x/d$ = 382 for $Re_{in}$ = 2176.

It is noted that this study is for the laminar mixed convective flow and heat transfer of $CO_2$ at supercritical pressures. During the computations we shall guarantee the laminar flow when the buoyancy force is involved. Jiang et al. [14] performed experimental and numerical studies of $CO_2$ in a 0.27 mm diameter microtube at supercritical pressures. Heating boundary condition was applied with inlet Reynolds numbers ($Re_{in}$) of 2900 and 1900. For $Re_{in}$ smaller than 2900, the local wall temperature varies non-linearly for both flow directions at high heat fluxes (113 kW/m$^2$). For the microtube used in their study, the buoyancy force effect is normally low even when the heating is relatively strong, while the flow acceleration due to heating can strongly influence the turbulence and reduce the heat transfer for high heat fluxes.

Table 1 shows the run parameters in this study with $Re_{in}$ in the range of 930–2176. Different from the studies by Jiang et al. [14], this study used the cooling boundary condition on the wall. As noted above, the horizontal flow behaves the strongest buoyancy

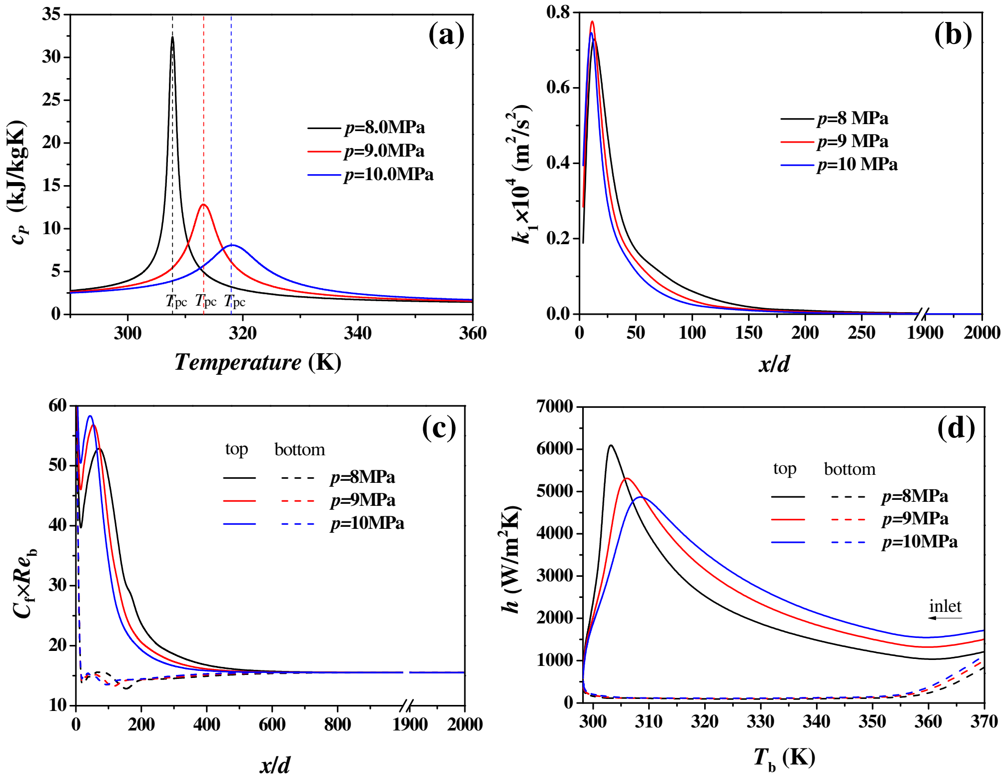


**Fig. 17.** Effect of pressures on the specific heat of $CO_2$ (a), kinetic energy of secondary flow (b), $C_f \times Re_b$ (c), and heat transfer coefficient (d) for run 2 at ($\alpha = 0^{\circ}$).

force effect among all the inclination angles. Fig. 16 plotted Reynolds number vs. bulk fluid temperatures at three wall temperatures for runs 1, 5 and 8 for horizontal flow. It is seen that local Reynolds numbers are decreased from large to low bulk fluid temperatures. In summary, the laminar flow is ensured by using low inlet Reynolds number, as well as by the reduced Reynolds numbers along the flow direction due to the cooling boundary condition.

### 3.3. Effect of pressures on the flow and heat transfer

The above computations focus on the pressure of 8.0 MPa, which is close to the critical pressure of 7.38 MPa for $CO_2$. Real applications of compact heat exchangers may deviate from the pressure of 8.0 MPa. Here we discuss the pressure effect on the laminar mixed convective flow and heat transfer. Fig. 17a shows the specific heats vs. $CO_2$ temperatures. The pseudocritical temperatures ($T_{pc}$) are shifted to larger temperatures with increases in pressures. Meanwhile, the maximum specific heats are decreased with increases in pressures. The specific heat, as well as other physical property variations vs. pressures, cause the change of flow and heat transfer behavior deviating from $p = 8.0$ MPa. Fig. 17b–d show the kinetic energies of secondary flow, friction factors and heat transfer coefficients with pressures of 8–10 MPa. All the three pressures share similar trends for these parameters. The increased pressures slightly decrease the kinetic energies of secondary flow. Further flow development evolves very small kinetic energies at the flow downstream (see Fig. 17b). Fig. 17c shows that friction factors at the top generatrix points are increased to a peak value and then decreased. The maximum friction factor appears at the pseudocritical temperature. The increased pressures increase the friction factors for small $x/d$, but decrease the friction factors for large $x/d$ beyond the pseudocritical temperature. The friction factors at the bottom generatrix points are not changed by pressures.

The heat transfer coefficients are changed by pressures apparently (see Fig. 17d). At low bulk fluid temperatures ($T_b < T_{pc}$), high pressures decrease the heat transfer coefficients. But high pressures increase the heat transfer coefficients at larger bulk fluid temperatures ($T_b > T_{pc}$). The peak heat transfer coefficients are decreased from 6103 W/m$^2$ K at $p = 8.0$ MPa to 4880 W/m$^2$ K at $p = 10.0$ MPa.

## 4. Conclusions

We performed the numerical simulations of mixed convective flow and heat transfer in a 0.5 mm diameter and 1000.0 mm length tube. The following conclusions can be drawn:

- Temperatures are significantly non-uniform for inclined flows at the tube entrance, which are higher at the upper part and lower at the bottom part of the tube cross section. The non-uniform degree is improved with flow development. The thermally developed flow at inclined conditions and vertical flows behave the uniform temperature distributions.
- Velocity contours are distorted with higher values at the upper part and lower values at the bottom part of the cross section for horizontal and inclined flows at the tube entrance. The fully develop flow behaves the parabolic velocity curve. The kinetic energies of the secondary flow are larger for the horizontal and inclined flows. They approach zero for the vertical upward and downward flows.
- The vertical upward and downward flows yield smallest and largest $C_f \times Re_b$ values respectively. The $C_f \times Re_b$ values at the bottom generatrix point are decreased with increases in inclination angles, and attain the value of 16 for the fully develop flow.

- The heat transfer coefficients are significantly larger at the top generatrix point than those at the bottom generatrix point with the inclination angles of $-60°$–$60°$. The horizontal flow and slightly inclined flows ($\alpha = -30°$ and $30°$) behave larger heat transfer coefficients.
- The heat transfer performance is best under the earth environment. The effect of inclination angles on the heat transfer is decreased with decreases in the gravity force magnitudes. This effect can be neglected at micro gravity of $9.81 \times 10^{-4}$ m/s$^2$.

## Acknowledgement

This work was supported by the Natural Science Foundation of China with the contract numbers of 51006035 and U1034004, and by the Natural Science Foundation of China of International cooperation project (51210011).

## References

[1] P.X. Jiang, C.R. Zhao, R.F. Shi, Y. Chen, W. Ambrosini, Experimental and numerical study of convection heat transfer of $CO_2$ at super-critical pressures during cooling in small vertical tube, Int. J. Heat Mass Transfer 52 (2009) 4748–4756.
[2] X.L. Cao, Z.H. Rao, S.M. Liao, Laminar convective heat transfer of supercritical $CO_2$ in horizontal miniature circular and triangular tubes, Appl. Therm. Eng. 31 (2011) 2374–2384.
[3] Z.H. Li, P.X. Jiang, C.R. Zhao, Y. Zhang, Experimental investigation of convection heat transfer of $CO_2$ at supercritical pressures in a vertical circular tube, Exp. Therm. Fluid Sci. 34 (2010) 1162–1171.
[4] R.P. Bringer, J.M. Smith, Heat transfer in the critical region, AIChE J. 3 (1957) 49–55.
[5] B.S. Shiralkar, P. Griffith, The deterioration in heat transfer to fluids at supercritical pressure and high heat fluxes Cambridge, Mass MIT Engineering Projects Laboratory, 1968, pp. 1–180.
[6] R.C. Hendricks, R.J. Simoneau, R.V. Smith, Survey of heat transfer to near-critical fluids, National Aeronautics and Space Administration, Washington DC, 1970, pp. 1–112.
[7] S. He, W.S. Kima, J.H. Bae, Assessment of performance of turbulence models in predicting supercritical pressure heat transfer in a vertical tube, Int. J. Heat Mass Transfer 51 (2008) 4659–4675.
[8] P.G. Debenedetti, R.C. Reid, Diffusion and mass transfer in supercritical fluids, AIChE J. 32 (1986) 2034–2046.
[9] J. Pettersen, R. Rieberer, S.T. Munkejord, Heat transfer and pressure drop for flow of supercritical and subcritical $CO_2$ in microchannel tubes, Eur. Res. Office US Army (2000).
[10] S.M. Liao, T.S. Zhao, Measurements of heat transfer coefficients from supercritical carbon dioxide flowing in horizontal mini-micro channels, J. Heat Transfer 24 (2002) 413–420.
[11] S.M. Liao, T.S. Zhao, An experimental investigation of convection heat transfer to supercritical carbon dioxide in miniature tubes, Int. J. Heat Mass Transfer 45 (2002) 5025–5034.
[12] S.M. Liao, T.S. Zhao, A numerical investigation of laminar convection of supercritical carbon dioxide in vertical mini/micro tubes, Prog. Comput. Fluid Dyn. 2 (2002) 144–152.
[13] P.X. Jiang, Y. Zhang, R.F. Shi, Experimental and numerical investigation of convection heat transfer of $CO_2$ at supercritical pressures in a vertical mini-tube, Int. J. Heat Mass Transfer 51 (2008) 3052–3056.
[14] P.X. Jiang, Y. Zhang, C.R. Zhao, R.F. Shi, Convection heat transfer of $CO_2$ at supercritical pressures in a vertical mini tube at relatively low Reynolds numbers, Exp. Therm. Fluid Sci. 32 (2008) 1628–1637.
[15] P.X. Jiang, Z.H. Li, C.R. Zhao, Convection heat Transfer of $CO_2$ at supercritical pressures in a vertical mini Tube, in: International Conference on Heat and Mass Transfer, Shanghai, China, 2009.
[16] S. He, P.X. Jiang, Y.J. Xu, R.F. Shi, W.S. Kim, J.D. Jackson, A computational study of convection heat transfer to $CO_2$ at supercritical pressures in a vertical mini tube, Int. J. Therm. Sci. 44 (2005) 521–530.
[17] Z.X. Du, W.S. Lin, A.Z. Gu, Numerical investigation of cooling heat transfer to supercritical $CO_2$ in a horizontal circular tube, J. Supercrit. Fluids 55 (2010) 116–121.
[18] J. Orfi, N. Galanis, C.T. Nguyen, Laminar fully developed incompressible flow with mixed convection in inclined tubes, Int. J. Numer. Meth. Heat Fluid Flow 3 (1993) 341–355.
[19] T. Walisch, M. Mtiller, W. Dorfler, C. Trepp, The heat transfer to supercritical carbon dioxide in tubes with mixed convection, High Press. Chem. Eng. (1996) 199–204.
[20] A.A. Busedra, H.M. Soliman, Experimental investigation of laminar mixed convection in an inclined semicircular duct under buoyancy assisted and opposed conditions, Int. J. Heat Mass Transfer 43 (2000) 1103–1111.
[21] A. Ozsunar, S. Baskaya, M. Sivrioglu, Experimental investigation of mixed convection heat transfer in a horizontal and inclined rectangular channel, Heat Mass Transfer 38 (2002) 271–278.
[22] H.A. Mohammed, Y.K. Salman, Combined convection heat transfer for thermally developing aiding flow in an inclined circular cylinder with constant heat flux, Appl. Therm. Eng. 27 (2007) 1236–1247.
[23] D.T. Chong, J.P. Liu, J.J. Yan, Effects of duct inclination angle on thermal entrance region of laminar and transition mixed convection, Int. J. Heat Mass Transfer 51 (2008) 3953–3962.
[24] E.W. Lemmon, M.L. Huber, M.O. McLinden, Reference fluid thermodynamic and transport properties (REFPROP). Version8.0, NIST Standard Reference Database 23, National Institute of Standard and Technology, Gaithersburg, MD, USA, 2007.
[25] F.B. Gessner, The origin of secondary flow in turbulent flow along a corner, J. Fluid Mech. 58 (1973) 1–25.
[26] S.S. Pital, D.M. Robinson, A. Zingerli, E.A. Groll, S. Ramadhyani, Heat transfer and pressure drop characteristics during in-tube gas cooling of supercritical carbon dioxide, American Society of Heating, Refrigerating and Air Conditioning Engineers Inc., 2000. pp. 93–96.
[27] W.B. Hall, Heat transfer near the critical point, Adv. Heat Transfer 7 (1971) 1–86.
[28] A. Bruch, A. Bontemps, S. Colasson, Experimental investigation of heat transfer of supercritical carbon dioxide flowing in a cooled vertical tube, Int. J. Heat Mass Transfer 52 (2009) 2589–2598.
[29] S.M. Yang, W.Q. Tao, Heat Transfer, fourth ed., Higher Education Press, Beijing, 2006. pp. 273–274 (Chinese edition).